13th Spring School on Transition and Turbulence
September 19th-23rd, 2022, Blumenau, SC, Brazil

EPTT-2022-0029
ANALYSIS OF THE LEAST STABLE EIGENVALUES IN THE TRANSITION FROM VORTEX-INDUCED VIBRATIONS TO GALLOPING

Victor Hugo Santiago Peron
Daiane Iglesia Dolci
Bruno Souza Carmo
Escola Politécnica da Universidade de São Paulo. Av. Professor Mello Moraes, 2231, Cidade Universitária, São Paulo - SP
victor.peron@usp.br
dolci@usp.br
bruno.carmo@usp.br

Abstract. *This works aims at performing linear stability analysis of fluid-structure interactions systems, focusing on aeroelastic bodies subject to vortex-induced vibrations, transverse galloping and pre-galloping. First, the physical phenomena behind these coupled instabilities are described, and the problem is set up to acknowledge the development of VIV and galloping in current fluid mechanic simulations. We take advantage of the moving frame of reference technique, allowing the rigid motion of the mesh, as well as the spectral\hp element discretization, to develop a solver that combines this high-order finite element method providing solutions with low numerical errors. We perform numerical nonlinear simulations of the flow around elastically mounted square cylinders to investigate the behavior of the coupled system and evaluate the system response with the variation of flow parameters (such as Reynolds number) and structural parameters (such as reduced velocity). Also, the methodology for modal stability analysis of the coupled systems is defined, and numeric simulations are carried out to obtain complementary sets of the leading eigenvalues responsible for the magnitude and oscillatory responses of these systems. These eigenvalues are determined as the solution for the perturbed coupled Navier-Stokes and structural equations, presented in the form of direct modes. Then, with a complete set of parameters, responses and respective eigenvalues, the fluid-structure stability is discussed in terms of the flow and structure parameters and geometry. We provide bifurcation diagrams, as well as the direct flow fields for the evolution or decay of the perturbation energy in the system.*

Keywords: *galloping, aeroelasticity, fluid-structure interactions, vortex-induced vibrations, modal stability analysis*

1. INTRODUCTION

The study of fluid-structure interaction (FSI) is a multi-physics science that fuses the knowledge of fluid and structural mechanics, investigating how solid and fluid parts of a domain of interest interact with one another. Once it deals with complex mechanics and a great number of variables, FSI problems rely mostly on experiments and numerical simulations. There are many ramifications of FSI, depending on the class of the flow (internal or external), compressibility of the fluid, production of sound, the kind of movement from the solid, stiffness and geometry of the solid, among a lot of other variables. This study focusses on aeroelasticity, defined as FSI instabilities derived from aerodynamic forces.

Cossu and Morino (2000), followed by Meliga and Chomaz (2011), provided linear stability analysis for an elastically mounted circular cylinder and analyzed the 2 main eigenvalues, defined as Fluid Mode (FM) and Elastic Mode (EM). Next, Navrose and Mittal (2016) continued with the eigenvalue analysis of a circular cylinder under VIV and defined how the fluid mode and the elastic mode change with the variation of the mass ratio. For high values of mass ratio, there are two distinct FM and EM modes, each with independent behavior. On the other hand, for low mass ratio systems, both FM and EM interact, creating two fluid-elastic modes (FEMI and FEMII), and each one contributes more to the behavior of the system for specific ranges of reduced velocities. Also, contributing to the lock-in region analysis, Singh and Mittal (2005), proved that this region is characterized by a proximity between the vortex-shedding and the cylinder natural frequencies.

Dolci (2020) extended this analysis for the moving frame of reference using the Spectral/*hp* discretization technique, validating the study of Navrose and Mittal (2016) in this particular framework and included the background for nonlinear simulations.

Li et al (2019) extended the eigenvalue analysis for the galloping instability and found that, for that case, there must always be a fluid-mode that remains stable (FMI), and the EM interacts (for low mass ratio systems, decoupled) with a second fluid mode, FMII. Also, they verified that SM turns unstable inside the lock-in region and remains nearly constant for the entire pre-galloping and galloping regime. It proves that, in the pre-galloping state, FMI is still the greatest

contributor to the system and the instability of SM still does not play such a decisive role. Also, in the galloping regime, they showed that the main responsible for the dynamics of the system is the instability of SM.

The present work seeks to extend the work of Li et al (2019), providing VIV and galloping analysis for systems with lower and higher values of Reynolds numbers, seeking to investigate the response of the SM mode dynamics and its relationship with the aeroelastic stability.

The next section will cover all the theory behind these aeroelastic instabilities, the non-inertial frame of reference used and the modal stability analysis. In section 3, the methodology will be discussed and all the tools to perform the analysis will be demonstrated. Later, the results will be presented.

2. PROBLEM FORMULATION

2.1 Fundamentals

Vortex-induced vibrations is a fluid-structure instability that is triggered by vortex shedding loads, leading to vibrations. Some of the distinct characteristics of VIV is that it happens in a range, with a specific starting and ending point, and that it can indeed occur in circular cylinders (while other fluid-induced vibrations such as galloping cannot). This instability range, which is close to the natural frequency of the structure f_n and is named lock-in region, will be further explored in section 2.3.

Vortex shedding generates a time-periodic pressure distribution variation in both upper and lower boundaries, as seen in Figure 1. Once the instantaneous pressure distribution is generally not symmetric, it is possible to infer that there is an equivalent oscillating lift force occurring in the body, defining a self-lift mechanism. Also, the event of vortex shedding is seen in a range of fluid velocities and have different laminar and turbulent characteristics.

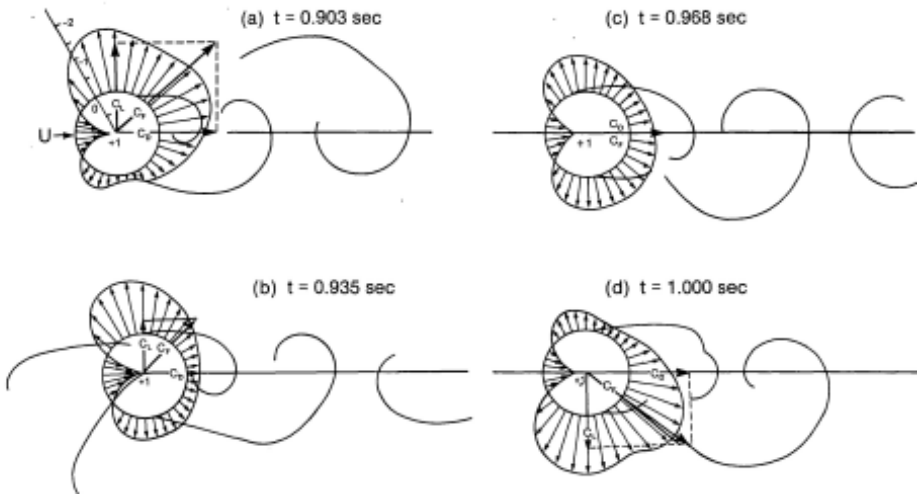

Figure 1 - Sequence of surface pressure fields and wake patterns in different time-steps. Extracted from Blevins (1990)

The event of transverse galloping is schematically shown in Figure 2, which shows the flow response to a vertical perturbation. Consider a generic bluff body under crossflow that slowly starts vibrating and has a downwards vertical velocity $\dot{y}$. If the geometry is fixed the flow is responsible for generating the aerodynamic forces. However, when the bodies undergo a small perturbation motion generating a transverse velocity, it also contributes to the final forces. The reason behind it is due to the relative velocity $\mathrm{U_{rel}} = \mathrm{U} + \dot{y}$ that is responsible for generating the fluid forces. Note the spring of stiffness k and the damping coefficient c used to generically demonstrate the attachment of the body to a fix reference.

Galloping is a self-excited instability that generates a bifurcation point, unlike VIV, therefore it only has a starting point, and the instability does not cease with the increment of the flow parameters (such as Reynolds number or reduced velocity).

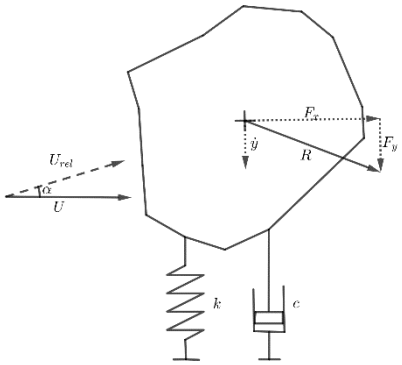

Figure 2 - Generic convex body in the onset of Galloping

Both VIV and transverse galloping are governed by differential equations which, for the study of circular cylinders (VIV only), is defined as:

$$\frac{\pi}{4}\ddot{y} + \frac{\pi^2\zeta}{U_R}\dot{y} + \frac{\pi^3}{U_R^2}y = \frac{1}{m^*}F_y \tag{1}$$

While, for square cylinders (containing both VIV and galloping):

$$\ddot{y} + \frac{2\zeta}{U_R}\dot{y} + \left(\frac{1}{U_R}\right)^2 y = \frac{1}{m^*}F_y \tag{2}$$

In these equations, the y terms and its time derivatives denote the position, velocity and acceleration of the body, F_y denotes the vertical non-dimensional force per unit span, ζ denotes the damping ratio and, finally, U_R and m^* defines the FSI main dimensionless parameters, the reduced velocity and the mass ratio.

The mass ratio, which describes the differences between equation (1) and (2), is the relation between the mass of the solid and the displaced mass of fluid and it is defined as $m^* = \frac{\widetilde{m_s}}{\widetilde{m_f}} = \frac{4\widetilde{m_s}}{\tilde{\rho}\pi\widetilde{D^2}}$ for a circular cylinder and $m^* = \frac{\widetilde{m_s}}{\widetilde{m_f}} = \frac{\widetilde{m_s}}{\tilde{\rho}\tilde{h}^2}$ for square prisms, considering $\widetilde{m_s}$ and $\widetilde{m_f}$ the dimensional mass of the solid and the fluid, $\tilde{\rho}$ the fluid density, $\tilde{h}$ the square side and $\widetilde{D}$ the circular cylinder diameter. The reduced velocity, for both motions, is the relation between the free-stream velocity of the fluid and a characteristic velocity of the body, defined as $U_R = \frac{U_0}{\tilde{w}f_n}$, with $\tilde{w}$ being a characteristic length ($\tilde{h}$ for square and $\widetilde{D}$ for circular cylinder).

2.2 Moving Frame of Reference

The moving frame of reference, pioneered by Li, Sherwin and Bearman (2002), is a technique that allows the simulation of Fluid-Structure Interaction systems for rigid body motions by changing the frame of reference from an inertial absolute frame to the body reference (non-inertial). Let $x_{a,1}$ and $x_{a,2}$ be, respectively, the horizontal and vertical axis in the absolute frame of reference and x_1 and x_2 orthogonal axes in the moving frame of reference, standing with its origin in the the center of the body (since the body is not allowed to rotate in this study, there is no need to define the point as the shear center or the centroid). The transformation for each of the coordinate is defined as $\boldsymbol{x} = \boldsymbol{x_a} - \mathrm{y}$ and presented in Figure 3. The time derivative of the change of coordinates is equal to:

$$\boldsymbol{u} = \boldsymbol{u_a} - \dot{y} \tag{3}$$

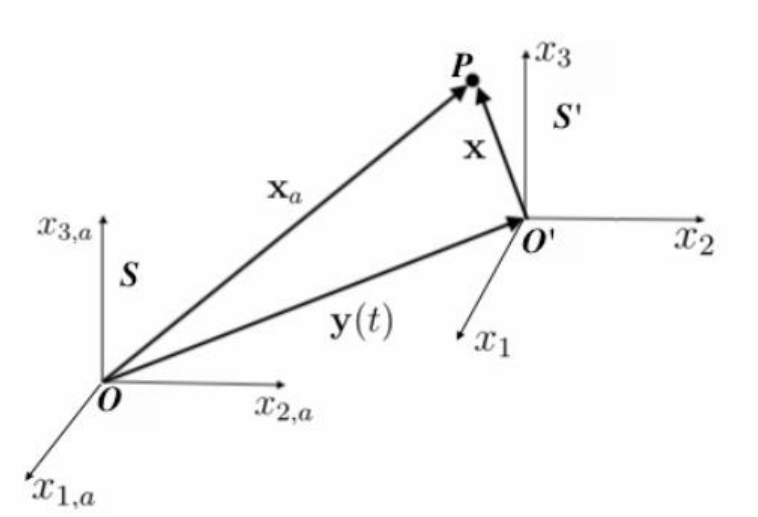

Figure 3 - Moving Frame of Reference Mapping Scheme. Extracted from Dolci (2020)

Proceeding with the motion of the body and transforming the Navier-Stokes equations from the absolute to the moving frame of reference, for the square cylinder analysis, the final coupled system for direct NS simulations is defined as:

$$\frac{\partial \boldsymbol{u}}{\partial t} + \nabla \boldsymbol{u} \cdot \boldsymbol{u} - \frac{1}{Re}\nabla^2 \boldsymbol{u} + \nabla p + \frac{d\dot{y}}{dt} = 0 \tag{4a}$$

$$\nabla \cdot \boldsymbol{u} = 0 \tag{4b}$$

$$\ddot{y} + \frac{2\zeta}{U_R}\dot{y} + \left(\frac{1}{U_R}\right)^2 y = \frac{1}{m^*}F_y \tag{4c}$$

Subjected to the boundary conditions of $\boldsymbol{u} = 0$ at the structure walls, equation (3) for the inlet and $\nabla \boldsymbol{u} \cdot \boldsymbol{n} = 0$ at the outlet.

2.3 Modal Stability Formulation

Linearizing the system of equation (4) for all state variables $\boldsymbol{q} = [u, v, p, y, \dot{y}]$ considering a small perturbation of the form $\boldsymbol{q} = \boldsymbol{Q} + \boldsymbol{q}'$ where $\boldsymbol{Q}$ denotes the steady base flow variables and $\boldsymbol{q}'$ a small perturbation, it is possible to arrive at a new set of equations to analyze the evolution of the perturbation using modal analysis. The complete set of equations for this work was developed by Dolci (2020). A modal stability analysis consists of an eigenvalue analysis of the linear operator of the FSI system L, assuming:

$$(\lambda \mathbf{I} - \mathrm{L})\hat{\mathbf{q}} = 0$$

Since stability FSI analysis seeks mainly for the onset of the instability, it is enough, in most cases, to evaluate only the least stable eigenvalues. The stability analysis used in this study has its eigenvalues determined using the Modified Arnoldi Method (defined in section 3.3) and provide the final solution approximated by normal modes, such as $\boldsymbol{q}' = \hat{\boldsymbol{q}}\boldsymbol{e}^{\lambda t}$. The eigenvalue λ is an imaginary number of the form $\lambda = \lambda_r + i\lambda_i$ where the real part determines the perturbation magnitude (its growth or decay), and the imaginary part defines the periodic oscillation. Therefore, to ensure stability, it is important to state that the growth is smaller than 1, since it is a multiplier of $\hat{\mathbf{q}}$. Therefore, for stability,

$\mathrm{M} = \mathrm{e}^{\lambda_r}$,
$\mathrm{M} = \mathrm{e}^{\lambda_r} < 1$,
$\ln \mathrm{M} = \ln \mathrm{e}^{\lambda_r} < \ln 1$,
$\ln \mathrm{M} = \lambda_r < 0$

So, the stability is ensured in a modal analysis if the least stable eigenvalues have a negative real part. As discussed by Li et al (2019), the interaction of the 3 least stable eigenvalues defines the stability for galloping. The final FSI coupled system for the linear stability analysis is defined by:

$$\lambda\hat{\boldsymbol{u}} + \nabla\boldsymbol{U}\cdot\hat{\boldsymbol{u}} + \nabla\hat{\boldsymbol{u}}\cdot\boldsymbol{U} - \frac{1}{Re}\nabla^2\hat{\boldsymbol{u}} + \nabla\hat{p} = 0 \tag{5a}$$

$$\nabla\cdot\hat{\boldsymbol{u}} = 0 \tag{5b}$$

$$\lambda\hat{y} - \widehat{y_1} = 0 \tag{5c}$$

$$\lambda\widehat{y_1} + \frac{4\pi\zeta}{U_R}\widehat{y_1} + \left(\frac{2\pi}{U_R}\right)^2\hat{y} - \frac{1}{m^*}F_y = 0 \tag{5d}$$

Subjected to the boundary conditions of $\hat{\boldsymbol{u}} = 0$ in the inlet, $\nabla\hat{\boldsymbol{u}}\cdot\boldsymbol{n} = 0$ in the outlet and $\hat{\boldsymbol{u}} = \widehat{y_1} - \nabla\mathbf{U}\varphi$ in the structure wall, where φ is the small perturbation in the crossflow direction. It is important to state that, as developed by Dolci (2020), the correct evaluation of these equations must include an added stiffness term, which vanishes in this analysis due to the symmetry of the base flow and the assumption of a rigid body motion, which excludes alterations in the forces due to alterations in the geometry.

3. METHODOLOGY

3.1 Spectral/*hp* Element Method Disctretization

Throughout this study, all numerical simulations are executed employing the spectral/*hp* element method (SEM), developed by Karniadakis and Sherwin (2005) which is a method for solving partial differential equations. This method is used to solve the Navier-Stokes equations and the coupled fluid-structure interaction problems.

SEM is a method that unites techniques from two other numerical methods, the finite element method (FEM) and the spectral method (SM), in order to merge the benefits from both and to be able to solve numerical problems with high accuracy and less computational power. SEM merges both techniques in one, applying both the convergences *h* and *p*. Therefore, SEM also defines a discrete set of elements that represents the original geometry, and inside every element the behavior of the system is interpolated by a high-order polynomial basis. Different polynomial basis can be defined, but for numerical reasons it is convenient that the basis is at least approximately orthogonal. The most common basis used in SEM are the Jacobi polynomial basis and the Lagrange nodal basis. The present work is developed employing the Jacobi basis.

3.2 Newmark-β Method

Newmark-β is a method to solve second-order ordinary differential equations. This approach can assume two frameworks. In the first one, during a time-step $\Delta\mathrm{t} = \mathrm{t_{n+1}} - \mathrm{t_n}$ the acceleration is assumed constant and in the second one as a linear function. The first case will be defined below, but the second can also be easily defined. This framework will generically adopt the variable x.

Assuming a constant acceleration defined as the mean of the acceleration in both time-steps and integrating two times, the result is

$$\ddot{\mathrm{x}} = \frac{1}{2}(\ddot{\mathrm{x}}_{\mathrm{n+1}} + \ddot{\mathrm{x}}_{\mathrm{n}}), \tag{11a}$$

$$\dot{\mathrm{x}} = \dot{\mathrm{x}}_{\mathrm{n}} + \frac{\mathrm{t}}{2}(\ddot{\mathrm{x}}_{\mathrm{n+1}} + \ddot{\mathrm{x}}_{\mathrm{n}}), \tag{11b}$$

$$\mathrm{x} = \mathrm{x_n} + \dot{\mathrm{x}}_{\mathrm{n}}\mathrm{t} + \frac{\mathrm{t}^2}{4}(\ddot{\mathrm{x}}_{\mathrm{n+1}} + \ddot{\mathrm{x}}_{\mathrm{n}}). \tag{11c}$$

It is possible to define the velocity and position in the time-step $\mathrm{t_{n+1}}$ simply as

$$\dot{\mathrm{x}}_{n+1} = \dot{\mathrm{x}}_n + \frac{\Delta\mathrm{t}}{2}(\ddot{\mathrm{x}}_{n+1} + \ddot{\mathrm{x}}_{n+1}), \tag{12a}$$

$$\mathrm{x_{n+1}} = \mathrm{x_n} + \dot{\mathrm{x}}_n\Delta\mathrm{t} + \frac{\Delta\mathrm{t}^2}{4}(\ddot{\mathrm{x}}_{n+1} + \ddot{\mathrm{x}}_n). \tag{12b}$$

Defining the second case (linear acceleration) and the first case, it is possible to generalize the results as

$$\mathrm{y_{n+1}} = \mathrm{y_n} + \delta\mathrm{t}\dot{\mathrm{y}}_{\mathrm{n}} + \frac{\delta\mathrm{t}^2}{2}[(1-2\beta)\ddot{\mathrm{y}}_{\mathrm{n}} + 2\beta\ddot{\mathrm{y}}_{\mathrm{n+1}}], \tag{13a}$$

$$\dot{y}_{n+1} = \dot{y}_n + \delta t[(1-\gamma)\ddot{y}_n + \gamma\ddot{y}_n + 1]. \tag{13b}$$

Since in this work the first approach of constant acceleration is used, to ensure numerical stability it is employed

$\beta = \frac{1}{4}$ and $\gamma = \frac{1}{2}$.

3.3 Arnoldi Method

When trying to obtain the eigenvalues and eigenvectors of matrices, the two main classes of algorithms used are the classical QZ and the projection methods. For the purposes of this study, the second one is more interesting because the matrices are large but not explicitly assembled, and we are interested in a very small part of the spectrum only. Projection methods use less computational power, with the cost of not providing the full spectrum of eigenvalues.

The Modified Arnoldi Method relies on the *Krylov* subspace to approximate the original matrix A by a superior Hessenberg matrix H_m, close to triangular. The eigenvalues and eigenvectors of H_m provide an accurate estimation of the least stable eigenvalues and eigenvectors of A. A complete understanding of this method can be found in Trefethen and Bau (1997).

3.4 Mesh Validation

To ensure the effectiveness of this study, a mesh convergence analysis was provided. Taking the example of the convergence in Li et al (2019), the first analysis was a comparison of the aerodynamic forces of a fixed square under flow. Two meshes were provided, denoted $MESH_1$ and $MESH_2$, both with external sizing $-50\tilde{h} \leq x, y \leq 50\tilde{h}$, with $MESH_1$ with 4407 elements and $MESH_2$ with 4831. Table 1 provides a comparison with both meshes and a p convergence.

Table 1 - p convergence analysis for fixed square

Mesh	Polynomial Order	Strouhal	%St	CD_{med}	$\%CD_{med}$	CL_{rms}	$\%CL_{rms}$	Simulation Time (h)
1	5	0.1425	0.52%	1.4547	1.37%	0.1799	0.66%	9.05
1	6	0.1425	0.52%	1.4492	0.99%	0.1794	0.94%	11.74
1	7	0.1425	0.52%	1.4466	0.81%	0.1795	0.88%	16.89
2	5	0.1425	0.52%	1.4523	1.21%	0.1796	0.83%	9.87
2	6	0.1425	0.52%	1.4478	0.89%	0.1793	0.99%	12.78
2	7	0.1425	0.52%	1.4455	0.73%	0.1795	0.88%	18.35
Ref	-	0.1432	0.00%	1.435	0.00%	0.1811	0.00%	-

This analysis defined the polynomial order as $P = 6$, since it is within 1% of the reference mesh. Next, to decide whether $MESH_1$ or $MESH_2$ is best suitable to the problem, a direct Navier-Stokes analysis was performed, considering a square cylinder under galloping with high amplitude. This was achieved considering the case studied by Robertson et al. (2003), considering $Re = 250$, $\zeta = 0.0037$, $U_R = 40$ and $m^* = 20$. Figure 4 provides the comparison between both meshes and the reference. Since there is visible alteration in the nonlinear behavior between $MESH_1$ and $MESH_2$ and both predict the behaviour with good accuracy, $MESH_1$ was defined as the final mesh due to its lower computational cost.

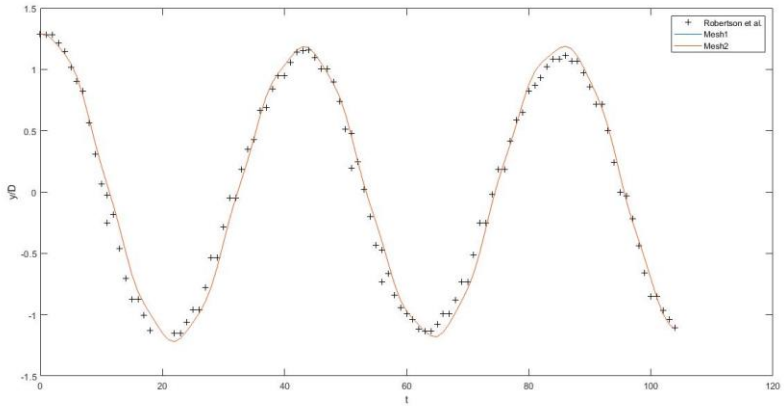

Figure 4 - Convergence of both meshes with nonlinear simulation from Robertson et al. (2003)

4. RESULTS

Li et al. (2019) defined the competition between the fluid and elastic modes for galloping analysis and defined that, in high mass ratio systems, the FMII mode and the SM mode are decoupled, which provides a clearer understanding of the mechanism of galloping. In those systems, the SM mode turns unstable while on the VIV regime and keeps unstable through the pre-galloping regime until galloping occurs.

Taking that into consideration and taking a PSD analysis of pre-galloping systems, Li et al. (2019) concluded that the pre-galloping regime is an instability caused by FMI (also simply denoted FM mode, for decoupled systems), without interference from SM (despite SM being unstable already in pre-galloping). Galloping, on the other hand, is indeed caused only by the unstable SM mode.

To evaluate these conclusions, this work first presents the results of direct Navier-Stokes simulations for a chosen range of Reynolds Numbers and evaluates the VIV and Galloping regimes. The chosen set of Re for these simulations are defined as $Re = \{75, 100, 150, 200\}$, covering the main regions of the simulation. $Re = 75$ seeks a flow that is only susceptible to VIV, with no pre-galloping regime. $Re = 100$ aims in displaying simulations with a pre-galloping regime but without galloping, and both $Re = 150$ and $Re = 200$ displays regions in which galloping does indeed occur but, while the first has only 2D instabilities for a fixed square, the second would also contain 3D instabilities, according to Saha et al. (2003). However, since the 2D instabilities are dominant from the 3D for $Re = 200$ (once it is close to the neutral 3D stability), it is possible to assume 2D simulations in that case. Figure 5 displays the amplitude of oscillation for a range of reduced velocities.

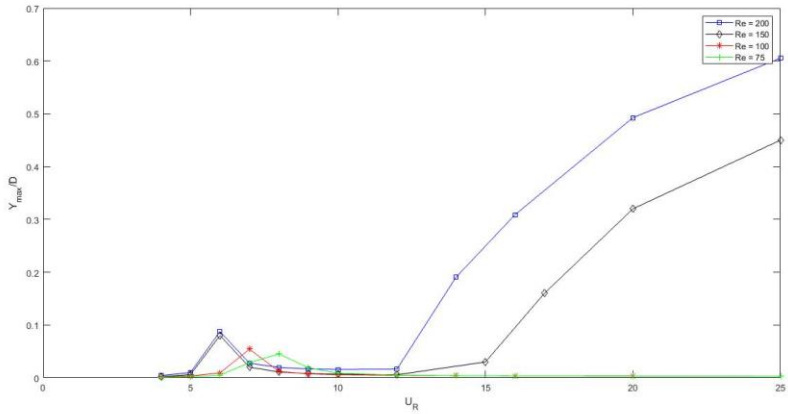

Figure 5 - Evolution of the amplitude of oscillation as a function of the reduced velocity for a range of Reynolds numbers

Next, linear stability analysis were performed for the same set of Reynolds numbers, including the value of $Re = 180$. This addition is intended to seek any differences in the behavior of the system in the 3D instability range. Figure 6 shows the variation of the FM and SM modes in relation to a set of reduced velocities.

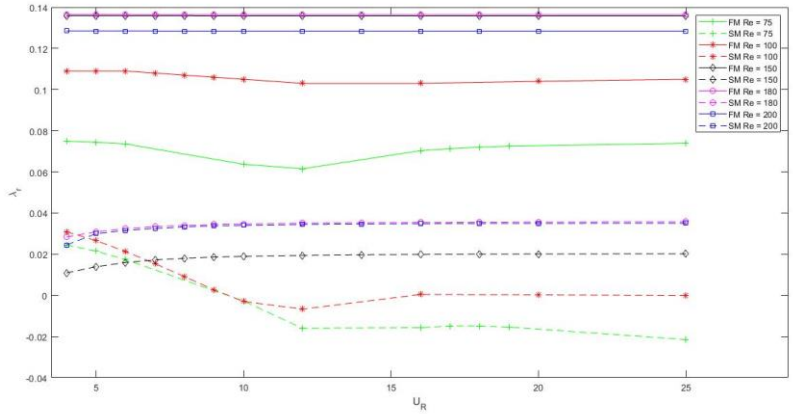

Figure 6 - Evolution of the real part of the 2 least stable eigenvalues for a range of Reynolds numbers

Also, for the SMs that present Galloping, Figure 7 presents the variation of the eigenfrequencies $\lambda_i/2\pi$ in relation to U_R.

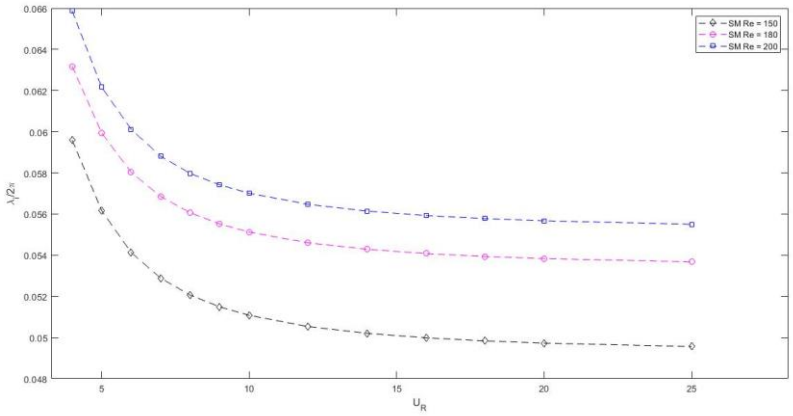

Figure 7 - Evolution of the eigenfrequencies for the subset of Reynolds numbers that present galloping

The results infer that, for a fixed mass ratio $m^* = 50$ throughout the entire study (providing a decoupled analysis and, therefore, only the 2 least stable eigenvalues are considered to the description of the system), an increase of the Reynolds numbers indicates that the onset of galloping occurs for a smaller value of reduced velocity and reaches higher amplitudes of oscillation for a fixed value of U_R. The linear stability analysis provides an understanding of the increase and decrease of the eigenvalues for different values of Reynolds number.

5. CONCLUSIONS

The numerical simulations performed, aligned with the considerations from Li et al. (2019) provided a framework for the investigation of the modes responsible for each range of instability (VIV, Pre-galloping ang Galloping). It was possible to confirm the assumptions that an unstable SM mode is responsible for both galloping and pre-galloping, with the difference being the oscillation frequency exiting the FM mode (or, in other words, the structure no longer oscillates in the vortex shedding frequency) and locking in the SM mode, indicating that the structure now oscillates according to its own frequency and demonstrating the self-excited phenomena of galloping.

Additionally, it is possible to infer that an increase in the Reynolds number also contributes to an increase in both the FM and SM modes, which enables the onset of galloping for a fixed value of reduced velocity. However, due to the surge of 3D instabilities for the higher values of Reynolds number, the value of FM and SM ceases to increase. However, the linear stability analysis in the present work could not obtain another positive real eigenvalue in this range (which could be the responsible for the 3D instability increase). 3D LSA analysis of this cases must be done to fulfill this gap.

6. REFERENCES

Blevins, R. D., 1990. *Flow-induced vibration*. Krieger Publishing Company, Malabar, 2nd edition.

Cossu, C. and Morino, L., 2000. "On the instability of a spring-mounted circular cylinder in a viscous flow at low Reynolds numbers". *Journal of Fluids and Structures* Vol.14, p. 183-196.

Dolci, D. I., (2020). *Adjoint-based stability and sensitivity analyses applied for fluid flow and fluid-structure interaction problems*. Ph.D. thesis, University of São Paulo, São Paulo.

Karniadakis, G. and Sherwin, S., 2005. *Spectral/hp element methods for computational fluid dynamics*. Oxford University Press on Demand.

Li, L., Sherwin, S.J. and Bearman, P.W., 2002. "A moving frame of reference algorithm for fluid/structure interaction of rotating and translating bodies". *International Journal for Numerical Methods in Fluids* Vol. 38, p. 187-206.

Li, X., Lyu, Z., Kou, J., & Zhang, W., 2019. “Mode competition in galloping of a square cylinder at low Reynolds number”. *Journal of Fluid Mechanics*, Vol. 867, p. 516-555.

Meliga, P. and Chomaz. J.M., 2011. "An asymptotic expansion for the vortex-induced vibrations of a circular cylinder". *Journal of fluid mechanics* Vol. 671, p. 137-167.

Navrose. and Mittal, S., 2016. “Lock-in in vortex-induced vibration”. *Journal of Fluid Mechanics*, Vol. 794, p. 565-594.

Robertson, I. et al., 2003. "A numerical study of rotational and transverse galloping rectangular bodies". *Journal of fluids and structures*, Vol.17, p. 681-699.

Saha, A. K. et al., 2003. " Three-dimensional study of flow past a square cylinder at low Reynolds numbers". *International Journal of Heat and Fluid Flow* Vol. 24, p. 54-66.

Singh, S. P. and Mittal, S., 2005. "Vortex-induced oscillations at low Reynolds numbers: hysteresis and vortex-shedding modes". *Journal of fluids and structures* Vol. 20, p. 1085-1104.

Trefethen, L. N. and Bau, D., 1997. *Numerical linear algebra*. Society for Industrial and Applied Mathematics, Philadelphia.

7. RESPONSIBILITY NOTICE

The authors are the only responsible for the printed material included in this paper.